Journal of Solid State Chemistry 183 (2010) 2731–2738

Contents lists available at ScienceDirect

Journal of Solid State Chemistry

journal homepage: www.elsevier.com/locate/jssc

Structural evolution of $Na_{0.5}K_{0.5}NbO_3$ at high temperatures

Nobuo Ishizawa [a,*], Jun Wang [a], Terutoshi Sakakura [a], Yumi Inagaki [b], Ken-ichi Kakimoto [b]

[a] Ceramics Research Laboratory, Nagoya Institute of Technology, Asahigaoka, Tajimi 507-0071, Japan
[b] Department of Materials Science and Engineering, Graduate School of Engineering, Nagoya Institute of Technology, Gokiso-cho, Showa-ku, Nagoya 466-8555, Japan

ARTICLE INFO

Article history:
Received 30 July 2010
Received in revised form
13 September 2010
Accepted 14 September 2010
Available online 18 September 2010

Keywords:
Sodium potassium niobate
$Na_{0.5}K_{0.5}NbO_3$
Single-crystal X-ray diffraction
Phase transition
Spontaneous polarisation
High temperature

ABSTRACT

Changes in structure and dielectric properties at elevated temperatures have been investigated on single-crystals of sodium potassium niobate, $Na_{0.5}K_{0.5}NbO_3$, grown by the flux method. Single-crystal X-ray diffraction studies revealed that the crystals underwent orthorhombic–tetragonal and tetragonal–cubic phase transitions at 465 and 671 K during heating and 446 and 666 K during cooling, respectively. Both transitions were accompanied by volumetric discontinuities of collapse upon heating and expansion upon cooling, suggesting that the transitions were of the first order. The coordination numbers of an Nb showed a decreasing tendency with decreasing temperature, i.e., 6 in cubic, 5+1 in tetragonal and 4+2 in orthorhombic. An Na atom occupied a slightly different position from the K atom in 12-fold coordination, resulting in fewer coordination numbers of 8+4 in cubic and tetragonal and 7+5 in orthorhombic. The spontaneous polarisation (P_s) estimated from the atom positions and formal charges were approximately 0.29 C m^{-2} in orthorhombic and 0.18 C m^{-2} in tetragonal. The contribution of the alkaline oxide components to P_s was estimated to be approximately 15% in both ferroelectric forms. The temperature-induced transitions were also confirmed through the dielectric constant and dielectric loss at various frequencies and the differential scanning calorimetry.

1. Introduction

Sodium potassium niobate $Na_{0.5}K_{0.5}NbO_3$ (NKN), and associated compounds containing various additional elements as dopants, are potential candidates for piezoelectric and ferroelectric applications, not only because of their high performance, but also their lead-free nature [1,2].

According to the phase diagram of $(Na_{1-x}K_x)NbO_3$, the orthorhombic *M* phase is stable in the range $0.475 \le x \le 1$, and the monoclinic *L* phase is stable in the range $0.32 \le x \le 0.475$, at room temperature [3]. The phase diagram in the range $0.24 < x < 0.36$ has been recently modified on the basis of monoclinic symmetry [4]. The *M* phase was assumed to have an orthorhombic symmetry from previous studies on the $x=1$ compound $KNbO_3$ (KN) [5–7]. However, although Li-doped NKN has been reported to have a monoclinic symmetry [8,9], no structural data for pure NKN is available to date in the inorganic crystal structure database [10].

The orthorhombic KN crystal undergoes a phase transition at *ca.* 493 K, and becomes paraelectric at *ca.* 707 K [11]. At these respective temperatures, the symmetry changes from orthorhombic to tetragonal (O–T) and from tetragonal to cubic (T–C). Heat treatment is known to sensitively affect the domain structure, which in turn influences the performance of devices utilizing KN or NKN [12,13]. Therefore, it is important to understand the crystallographic properties not only at the temperatures at which crystals are used in practical applications, but also at those temperatures at which crystals are treated during fabrication. In spite of many studies on the domain structures of an NKN at room temperature [14–20], it seems there is no crystallographic information available on an NKN at high temperatures, to the best of our knowledge.

The present study was then undertaken to elucidate the behaviour of the NKN structure at elevated temperatures, paying special attention to the changes in unit cell dimensions, atomic coordinates and bond distances. The present study also gives an estimate of the spontaneous polarisation (P_s) and its temperature dependence based on a simple point charge model.

The orthorhombic and tetragonal structures of KN were first described by the displacive model of constituent atoms with respect to the ideal cubic structure [5]. After this achievement, a series for the structural disorder of these structures was found [21–23]. Since then, a number of studies have been compiled on the basis of the displacive and order–disorder models from both experimental and theoretical points of view [6,7,24–29]. Today, the consensus seems to be that the displacive and the order–disorder natures are highly correlated, but that the latter becomes more prominent at higher temperatures.

To determine the temperature dependency of the NKN structure, diffraction data should be taken at a number of

* Corresponding author. Fax: +81 572 27 6812.
E-mail address: ishizawa@nitech.ac.jp (N. Ishizawa).

0022-4596/$ - see front matter © 2010 Elsevier Inc. All rights reserved.
doi:10.1016/j.jssc.2010.09.018

different temperatures. However, precise data collection at a single temperature takes a long time to accurately examine the order–disorder nature. Considering the aforementioned goal of the present paper, we decided to limit the time of data collection to 3 h at one temperature, which fully sufficed for the determination of structure based on the displacive model applied to the sublattices comprised of the Nb and O atoms. We believe the results of the present study also offer an insight into the full order–disorder nature of the compound.

Various cell choices have been adopted in the literature. However, the present paper follows the choice of Katz and Megaw [6]. The orientation relationships among the orthorhombic, tetragonal and cubic unit cells of an NKN adopted in this paper are shown in Fig. 1. The pseudocubic unit cell can be taken using cell vectors $\boldsymbol{a}_1$, $\boldsymbol{a}_2$ and $\boldsymbol{a}_3$, where $a_1=a_3$ and $\alpha=\gamma=90^\circ$ for the orthorhombic *Bmm*2 structure with the polar axis being parallel to $\boldsymbol{c}_o$. Because $\boldsymbol{c}_o$ is slightly longer than $\boldsymbol{a}_o$ in this setting, the β angle between $\boldsymbol{a}_1$ and $\boldsymbol{a}_3$ becomes smaller than 90°.

2. Experimental

2.1. Synthesis

NKN ceramics were prepared by a conventional mixed oxide method. The raw materials were high-purity (99.99%) powders of Na_2CO_3, K_2CO_3 and Nb_2O_5. These powders were weighed to obtain compositions according to the formula $Na_{0.5}K_{0.5}NbO_3$. The weighed powders were then mixed with ball-milling media for 1 h in ethanol. The dried mixture was calcined at 1073 K for 20 h.

Single-crystals were grown in air by the self-flux method. Briefly, the calcined powders were mixed with a KF–NaF eutectic composition. The weight ratio of the calcined powders, KF and NaF was 5:2:1. The weighed powders were then mixed by ball milling for 24 h in ethanol. The resulting mixture was put into Pt crucible and kept at 1323 K for 5 h, followed by cooling to 1223 K at the rate of 0.25 K/min. The sample was kept at 1223 K for 5 h, and then cooled to room temperature at the rate of 5 K/min.

The semi-quantitative energy dispersive X-ray spectroscopy analysis on the fragments of the crystal using a scanning electron microscope (JSM7000F, JEOL Ltd.) indicated that the Na/K ratios lay between 0.8–1.2. The relatively large variations were supposedly due to the residual flux components of KF and/or NaF on the surface of the crystals. On the other hand, the ratios converged to 0.9–1.1 by the population analysis of the single-crystal X-ray diffraction data. The Na/K ratio was eventually fixed at 1.0 in further calculations.

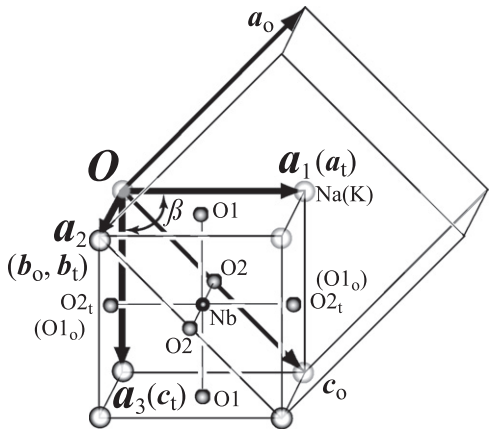

Fig. 1. Relationships among the orthorhombic *Bmm*2 unit cell (a_o, b_o, c_o), tetragonal *P*4*mm* cell (a_t, b_t, c_t) and the pseudocubic unit cell (a_1, a_2, a_3, β) with a schematic atom arrangement. Atom labels with no subscripts are common for the orthorhombic and tetragonal forms.

2.2. Diffraction experiments

Single-crystal diffraction experiments were carried out on a CCD diffractometer (Smart Apex II, Mo*K*α, Bruker AXS) with a heating apparatus [30]. A mono-capillary collimator 300 μm in diameter was used to enhance the diffracted intensities [31]. Crystals were ground into spheres 80 μm in diameter and mounted on the silica glass capillary by Sauereisen cement (#970000, Niraco Co.). The crystal on the diffractometer was heated by hot nitrogen gas flowing at the rate of 5 L/min. The sample temperature was calibrated by measuring the melting points of Sn, Zn, Al and Ag metals.

The intensity distribution in reciprocal space was investigated through the sets of contiguous frame data, so that more than 99% ($2\theta<60^\circ$) and 90% ($2\theta<80^\circ$) of all the crystallographically independent reflections were measured. Each set of frame data was taken by either the ω or φ scan techniques in scan steps of 0.3° with an exposure time of 3 s. In this way, it took 3 h to collect a set of frame data at one temperature. No diffraction spots were detected to break the *B*-centred orthorhombic symmetry at room temperature. The monoclinic distortion, as suggested for an Li-doped NKN [9], was thus excluded in the present crystal. Integrated intensities were extracted from the frame data by Smart Apex II software [32]. Absorption correction was applied by the empirical method using multiple reflections [32]. Least-squares refinements were carried out by the program SHELXL [33] in association with the WinGX program package [34].

A preliminary analysis at room temperature indicated that ferroelectric domains were present even in a tiny crystal *ca.* 30 μm in size, because many diffraction spots were faintly split or slightly extended in reciprocal space. The splitting in the NKN crystal was rather incomplete compared with the orthorhombic KN, owing to a small departure from cubicity. This was favourable for the single-crystal analysis assuming the pseudomerohedral twin. Tiny crystals with simple domain structures were selected from many candidates for the high temperature diffraction experiment. Details of the twin analyses are given in Sections 3.1 and 3.2.

Diffraction data were first taken at 10, 11 and 7 different temperatures in the orthorhombic, tetragonal and cubic forms, respectively, during heating the crystal from room temperature to 739 K. Then, additional diffraction data were taken at 7, 14 and 6 different temperatures in the cubic, tetragonal and orthorhombic forms, respectively, during cooling. Selected structure data at two representative temperatures upon cooling for orthorhombic, tetragonal and cubic forms are listed in Table 1. All the crystallographic information collected is available in the CIF archive as Supplementary material.

2.3. Dielectric properties and DSC measurements

The relative dielectric constant (ε') and the dielectric loss ($\tan\delta$) were measured in a furnace (KTF035N, Koyo Thermo System Co., Ltd.), using an LCR meter (ZM2355, NF Co.) on a platy crystal 1.29 mm thick. Data were taken for increasing and decreasing temperatures between 299 and 910 K at the rate of 5 K/min at frequencies of 0.1, 1, 10 and 100 kHz.

Thermal analysis of an NKN was performed using a differential scanning calorimeter (DSC-60, Shimadzu Co.). Data for the *ca.* 20 mg crushed sample were collected upon heating at the rate of 10 K/min in an Al cell under a nitrogen gas flow.

Table 1
Crystal data for an $Na_{0.5}K_{0.5}NbO_3$ at selected temperatures upon cooling.

T (K)	295	438	T (K)	474	648	T (K)	674	739
Crystal system	Orthorhombic		Crystal system	Tetragonal		Crystal system	Cubic	
Space group	*Bmm*2		Space group	*P*4*mm*		Space group	*Pm*$\bar{3}$*m*	
Z	2		*Z*	1		*Z*	1	
a_o (Å)	5.65732(18)	5.65576(19)	a_t (Å)	3.9767(2)	3.9868(1)	a_c (Å)	3.99281(8)	3.99433(8)
b_o (Å)	3.9551(12)	3.96668(13)						
c_o (Å)	5.67171(18)	5.66487(20)	c_t (Å)	4.0190(3)	4.0087(3)			
V_o (Å^3)	126.906(7)	127.089(7)	V_t (Å^3)	63.555(5)	63.716(4)	V_c (Å^3)	63.656(2)	63.728(2)
Pseudocubic unit cells before transformation								
a_1 (Å)	4.0054(1)	4.00245(10)	a_1 (Å)	3.9978(1)	3.9977(1)	a_1 (Å)	3.9924(1)	3.9943(1)
a_2 (Å)	3.9551(1)	3.96668(13)	a_2 (Å)	3.9767(2)	3.9868(2)	a_2 (Å)	3.9936(1)	3.9945(1)
a_3 (Å)	4.0054(1)	4.00245(10)	a_3 (Å)	3.9978(1)	3.9977(1)	a_3 (Å)	3.9924(1)	3.9943(1)
β (°)	89.854(3)	89.908(3)	β (°)	89.986(4)	89.993(4)	β (°)	89.999(3)	89.999(3)
V_{pc} (Å^3)	63.453(3)	63.545(4)	V_{pc} (Å^3)	63.555(5)	63.716(4)	V_{pc} (Å^3)	63.656(2)	63.728(2)
Refinements								
N_{all}[a]	658	649	N_{all}[a]	619	639	N_{all}[a]	659	658
R_{int}[b]	0.014	0.013	R_{int}[b]	0.021	0.022	R_{int}[b]	0.036	0.025
R_1[c]	0.021	0.018	R_1^c	0.017	0.017	R_1^c	0.019	0.014
N_{used}[d]	298	298	N_{used}[d]	224	226	N_{used}[d]	62	63
Structure parameters								
z(K)	−0.0160(4)	−0.0139(5)	z(K)	−0.0175(14)	−0.0156(15)	z(K)	0	0
U_{iso}(K)	0.0077(2)	0.0115(2)	U_{iso}(K)	0.0113(3)	0.0153(3)	U_{iso}(K)	0.0166(4)	0.0171(4)
z(Na)	0.008(3)	−0.002(5)	z(Na)	−0.002(10)	−0.003(10)	z(Na)	0.042(4)	0.062(2)
U_{iso}(Na)	0.0215(10)	0.0292(11)	U_{iso}(Na)	0.0345(19)	0.044(2)	U_{iso}(Na)	0.031(2)	0.020(2)
x(O1)	0.2488(6)	0.2467(7)						
z(O1)	0.2180(4)	0.2233(5)	z(O1)	−0.031(3)	−0.018(3)	z(O)	0	0
U_{iso}(O1)	0.0131(4)	0.0179(4)	U_{eq}(O1)	0.0214(17)	0.0253(12)	U_{eq}(O)	0.0204(3)	0.0201(4)
z(O2)	0.4613(5)	0.4651(5)	z(O2)	0.4685(17)	0.4763(18)			
U_{iso}(O2)	0.0088(5)	0.0122(5)	U_{eq}(O2)	0.0192(11)	0.0218(8)			
U_{eq}(Nb)	0.00733(4)	0.00966(4)	U_{eq}(Nb)	0.01164(7)	0.01360(6)	U_{eq}(Nb)	0.01554(7)	0.01636(8)
Selected interatomic distances (Å)								
Nb-O1 (× 2)	1.884(3)	1.911 (4)	Nb-O1	1.885 (12)	1.932 (12)	Nb-O	1.9964(1)	1.9972(1)
Nb-O1 (× 2)	2.131(3)	2.099 (3)	Nb-O1	2.134 (12)	2.076 (12)			
Nb-O2 (× 2)	1.9897(3)	1.9932 (3)	Nb-O2 (× 4)	1.9924 (4)	1.9957 (4)			
K-O1(× 4)	2.766(2)	2.772 (3)	K-O1(× 4)	2.8125 (3)	2.8191 (1)	K-O (× 12)	2.8233(1)	2.8244 (1)
K-O1(× 4)	2.865(2)	2.864 (3)	K-O2(× 4)	2.787 (6)	2.804 (7)			
K-O2(× 1)	2.707(4)	2.714 (4)	K-O2(× 4)	2.867 (6)	2.850 (7)			
K-O2(× 2)	2.8316(2)	2.8304 (2)						
K-O2(× 1)	2.965(4)	2.951 (4)						
Na-O1(× 4)	2.704 (9)	2.741 (12)	Na-O1(× 4)	2.814(2)	2.820(1)	Na-O (× 4)	2.707(10)	2.655(5)
Na-O1(× 4)	2.939 (10)	2.900 (12)	Na-O2(× 4)	2.74(3)	2.77(3)	Na-O (× 4)	2.8283(9)	2.8353(7)
Na-O2(× 1)	2.571(17)	2.65(2)	Na-O2(× 4)	2.91(3)	2.89(3)	Na-O (× 4)	2.944(12)	3.005(6)
Na-O2(× 2)	2.8410(16)	2.8340 (15)						
Na-O2(× 1)	3.101(17)	3.02(2)						

[a] Number of extracted reflections from the frame data.
[b] Mean reliability factor for equivalent reflections.
[c] Reliability factor of the least-squares refinement based on $F(hkl)^2$.
[d] Number of reflections used in the least-squares refinement.

3. Results and discussion

3.1. Refinements of the orthorhombic structure

Refinements were first undertaken to examine the domain structure of the orthorhombic crystal, assuming the presence of four domain components, 0, 1, 2 and 3. Domains 0 and 1 had the 90° relationship regarding the orientation of the polar axis and were geometrically related on the basis of the *Bmm*2 unit cell vectors, $\boldsymbol{a}_o$, $\boldsymbol{b}_o$ and $\boldsymbol{c}_o$ by the equation

$$\begin{pmatrix} \boldsymbol{a}_o \\ \boldsymbol{b}_o \\ \boldsymbol{c}_o \end{pmatrix}_1 = \begin{pmatrix} 0 & 0 & 1 \\ 0 & -1 & 0 \\ 1 & 0 & 0 \end{pmatrix} \begin{pmatrix} \boldsymbol{a}_o \\ \boldsymbol{b}_o \\ \boldsymbol{c}_o \end{pmatrix}_0 .$$

Domains 2 and 3, on the other hand, had the inversion relationship with domains 0 and 1, respectively. The volume fractions of domains 0, 1, 2 and 3 were estimated from the scale factors of these components in the course of the least-squares procedure under the constraint that the sum of the scale factors became unity.

The noncentrosymmetric refinement of the structure was carried out by fixing the fractional coordinate z of the Nb atoms at 0.5 along the polar axis. The positional and isotropic atomic displacement parameters of the Na and K atoms were refined independently. The z coordinates of O1 and O2 in Table 1 show that the oxygen sublattice shifted along the $-\boldsymbol{c}_o$ direction with respect to the Nb sublattice, which provided a net polarisation along $+\boldsymbol{c}_o$ in domain 0. The z coordinates of Na and K (Table 1) show that the Na sublattice shifted with respect to the oxygen sublattice further than the Nb sublattice shifted along $+\boldsymbol{c}_o$, whereas the K sublattice shifted the least. This phenomenon could be understood as follows: the Na cation in 12-fold coordination has an ionic radius of 1.39 Å, which is much smaller than the 1.64 Å radius of the K cation [35].

This discrepancy gave the Na atoms the attribute of rattling in the cavity surrounded by the corner-sharing NbO_6 octahedra. The small Na not only vibrated with large amplitude, as indicated by its atomic displacement parameter, but also shifted further from the centre of the cavity than K, resulting in a larger contribution to the total polarisation in the orthorhombic form. The contribution of the Na, K and Nb components to the total P_s will be discussed in Section 3.7.

3.2. Refinements of the tetragonal structure

The O–T transition turns one of the $\boldsymbol{a}_1$ and $\boldsymbol{a}_3$ cell vectors to $\boldsymbol{c}_t$, which is the unique axis of the tetragonal form (Fig. 1). When $\boldsymbol{a}_3$ turns into $\boldsymbol{c}_t$, the cell vectors $\boldsymbol{a}_1$ and $\boldsymbol{a}_2$ conform to the equivalent cell vectors $\boldsymbol{a}_t$ and $\boldsymbol{b}_t$ on the tetragonal basal plane. Depending on the choice of $\boldsymbol{a}_1$ and $\boldsymbol{a}_3$ for $\boldsymbol{c}_t$, two orientations are possible upon the O–T transition, resulting in the formation of 90° domains in the tetragonal crystal.

Peak splitting due to a small departure of the c_t/a_t ratio from unity was difficult to recognise in all crystals. The $\boldsymbol{a}_2$ corresponded to $\boldsymbol{b}_t$, whereas the a_1 and a_3 lengths showed an intermediate value between a_t and c_t, as given in Table 1, suggesting that the 90° domains developed over the crystal with the $\boldsymbol{a}_2$ axis in common. Therefore, the c_t length was calculated using the relationship $c_t = V_t/a_t^2 = a_1^2 a_2^{-1} \sin\beta$ from the refined pseudocubic cell. Intensity data were extracted from the frame data, assuming the same lattice as the orthorhombic form. They were then converted to the pseudocubic cell.

Four tetragonal domain components, 0–3, were first taken into consideration in the refinement, as done in the orthorhombic case. The domain components 0 and 1 had the following unit cell relationship:

$$\begin{pmatrix} \boldsymbol{a}_t \\ \boldsymbol{b}_t \\ \boldsymbol{c}_t \end{pmatrix}_1 = \begin{pmatrix} 0 & 0 & 1 \\ 0 & -1 & 0 \\ 1 & 0 & 0 \end{pmatrix} \begin{pmatrix} \boldsymbol{a}_t \\ \boldsymbol{b}_t \\ \boldsymbol{c}_t \end{pmatrix}_0 .$$

Components 2 and 3 had the inversion relationships with 0 and 1, respectively. The refinement eventually terminated with negligibly small fractions for domains 2 and 3. Further refinements were then carried out on the two-domain model. The volume ratio of domains 0 and 1 in the crystal was approximately 60:40 at all temperatures where the tetragonal form was stable. The positional and isotropic atomic displacement parameters of the Na and K atoms were refined independently as done in the orthorhombic case. The refined z coordinates of the Na atom and isotropic atomic displacement parameters showed similar tendency to those in the orthorhombic form.

3.3. Refinements of the cubic structure

Refinements of the structure in the cubic form were carried out after conversion from the B-centred orthorhombic lattice to the primitive cubic. Diffuse scattering was faintly observed running along the three $\langle 0\,0\,1 \rangle^*$ directions of reciprocal space. Difference Fourier synthesis showed a relatively large compilation of residual electrons around the origin which the Na and K atoms were first assumed to occupy randomly as in the ideal perovskite model. Various disorder models were then taken into consideration to explain these residuals. A final model was eventually adopted, in which the Na atom was assumed to statistically occupy the *Wyck*off 6*e* positions of the space group $Pm\bar{3}m$, whereas the K atom resided at the origin, 1*a*. The final model still indicated a small compilation of residual electrons around Nb in the difference Fourier maps; though their appearance varied at various temperatures where the cubic form was stable, and sometimes depended on the refinement strategy. Therefore, no further analysis was done in the present study.

3.4. Changes in cell volume

Changes in the unit cell volume of the orthorhombic, tetragonal and cubic forms induced by temperature are shown in Fig. 2, where the orthorhombic unit cell was reduced into the pseudocubic representation for comparison. The O–T and T–C transitions upon heating were detected at 465 and 671 K from volumetric discontinuities, respectively. The C–T and T–O transitions upon cooling were detected at 666 and 446 K, respectively. Disagreement between transition points upon heating and those upon cooling suggested that both transitions were of the first order.

The collapse of the pseudocubic unit cell volume upon the O–T and T–C transitions was 0.047% and 0.094%, respectively. This 1:2 volumetric relationship coincided with the ratio in the enthalpy change, i.e., 1.5 J/g for O–T and 3.0 J/g for T–C measured for NKN ceramics [36].

3.5. Changes in cell dimensions

Changes in cell dimensions with temperature are shown in Fig. 3. Upon the O–T transition, the orthorhombic $\boldsymbol{a}_1$ and $\boldsymbol{a}_3$ having the same length should split into the longer $\boldsymbol{c}_t$ and the shorter $\boldsymbol{a}_t$ in the tetragonal form, whereas the orthorhombic $\boldsymbol{a}_2$ should elongate and coincide with the tetragonal $\boldsymbol{b}_t$. The β angle between $\boldsymbol{a}_1$ and $\boldsymbol{a}_3$ was a variable in pseudocubic representation of the orthorhombic form, whereas it should become 90° in the tetragonal form if lattice strains due to twinning could be neglected. However, a very small deviation from 90° was

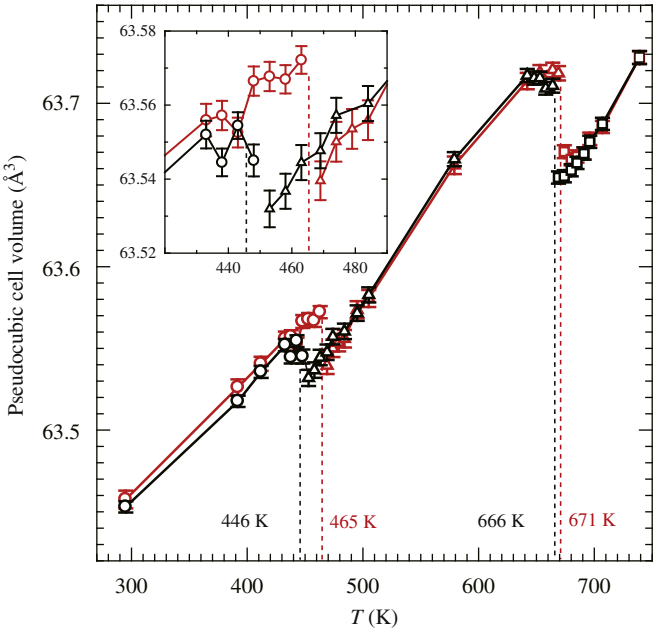

Fig. 2. Changes in the pseudocubic cell volume of $Na_{0.5}K_{0.5}NbO_3$ as a function of temperature with estimated standard uncertainties. The data points measured upon heating and cooling procedures are connected by red and black lines, respectively. The inset is an enlargement near the transition between the orthorhombic and tetragonal forms. The estimated phase transition points are given with vertical dashed lines upon heating (red) and on cooling (black). (For interpretation of the references to colour in this figure legend, the reader is referred to the web version of this article.)

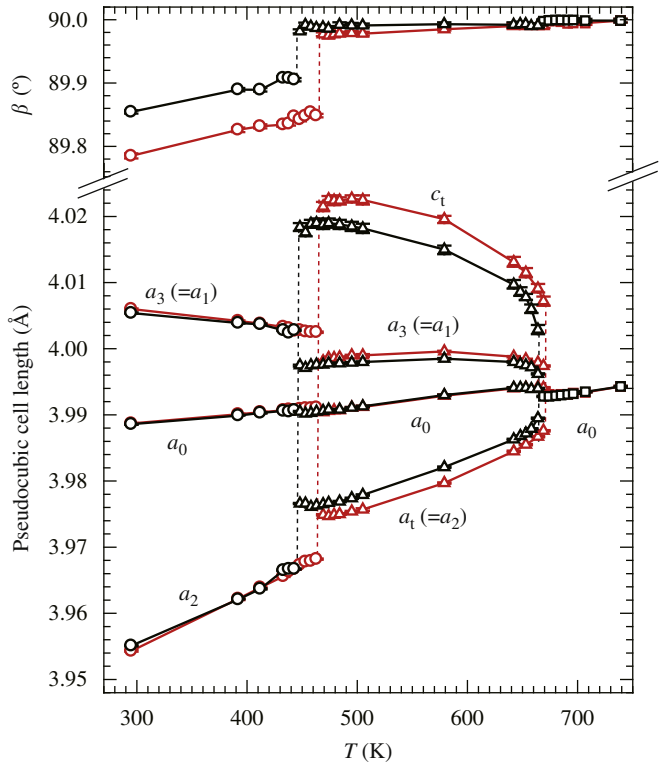

Fig. 3. Changes in cell dimensions of the orthorhombic (circle), tetragonal (triangle), and cubic (rectangle) forms as a function of temperature on heating (red) and on cooling (black), in terms of the pseudocubic unit cell characterized by $a_1(=a_3)$, a_2 and β. The reduced cell dimension, a_o, was calculated from $(a_1^2 a_2 \sin\beta)^{1/3}$. The tetragonal c_t was calculated from $a_1^2 a_2^{-1} \sin\beta$ (see text for details). The data points are connected by polylines for ease of view. The estimated standard uncertainties are drawn, though most of them are smaller than the markers. (For interpretation of the references to colour in this figure legend, the reader is referred to the web version of this article.)

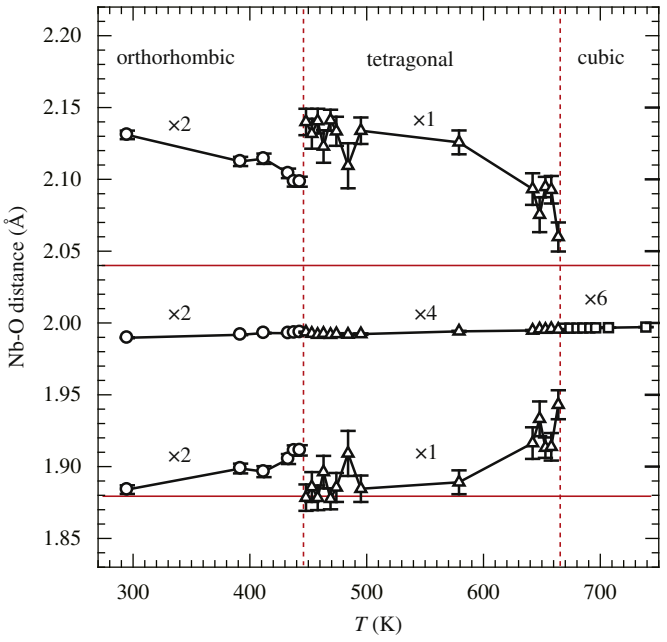

Fig. 4. Changes in Nb–O distances in $Na_{0.5}K_{0.5}NbO_3$ upon cooling. Data points with the estimated standard uncertainties are connected by solid lines for ease of view. The dashed vertical lines (red) indicate cubic–tetragonal and tetragonal–orthorhombic transition points upon cooling. The upper and lower horizontal lines (red) indicate the sum of ionic radii, $^{VI}Nb^{5+}+O^{2-}$ and $^{IV}Nb^{5+}+O^{2-}$, respectively. Number of equivalent distances is also indicated. (For interpretation of the references to colour in this figure legend, the reader is referred to the web version of this article.)

experimentally observed in the tetragonal form, and the a_1 and a_3 lengths were indistinguishable due to the 90° twinning.

The tetragonal cell dimensions changed almost quadratically with temperature in contrast to the linear-like behaviour of the orthorhombic ones. The tetragonal splitting, $[c/a-1]$, was 1.21% at 474 K when heated, which was significantly large compared with 1.06% at the same temperature upon cooling. The difference in $[c/a-1]$ between the heating and cooling procedures was almost constant throughout the temperature range where the tetragonal form was stable, suggesting that $[c/a-1]$ was subject to the domain structure brought into the C–T transition.

As shown in Fig. 3, a significant difference of *ca.* 0.06° in β was observed between heating and cooling, in contrast to the nearly reversible behaviours in the orthorhombic a_2 and $a_3(=a_1)$ dimensions. The difference in β between the heating and cooling procedures was almost constant at all temperatures where the orthorhombic form was stable, suggesting that it originated in the T–O transition. The smaller departure from 90° upon cooling might reflect the enhanced internal stress from the development of finer domains than those formed during heating.

3.6. Changes in interatomic distances

The temperature dependence of the Nb–O interatomic distance is shown in Fig. 4. The Nb–O distance could be classified into three types: *L* (~2.12 Å), *M* (~1.99 Å) and *S* (~1.90 Å). According to this classification, the orthorhombic form had two *L*, two *M* and two *S* distances, and the tetragonal form had one *L*, four *M* and one *S* distances, whereas the cubic form had six M distances.

Among them, the *L* distance could be eliminated from the coordination sphere of the Nb atom, because the *L* length was 0.08 Å longer than the sum of ionic radii, $^{VI}Nb^{5+}+O^{2-}$ (=2.04 Å) [35]. From this point of view, the C–T–O transitions upon cooling could be considered as a series of reductions in the coordination number for an Nb (i.e., 6 in cubic, 5 in tetragonal and 4 in orthorhombic, or at the least 5+1 in tetragonal and 4+2 in orthorhombic). If we further speculate the rhombohedral structure at lower temperatures, the coordination number would be 3, or 3+3 at the least. The stepwise change in coordination number for an Nb might reflect the nature of the first order phase transition.

The difference in ionic radii between Na and K affected the structure in various points of view. In all forms, as mentioned in Sections 3.1–3.3, Na and K occupied different positions with different atomic displacement parameters, which provided different interatomic distances for Na and K in structure (Table 1). At all temperatures investigated in three forms, the twelve K–O interatomic distances were less than the sum of ionic radii, $K^+ + O^{2-}$ (=3.04 Å) [35].

On the other hand, the Na atom was surrounded by 7 O at 2.57–2.84 Å, and extra 5 O at 2.94–3.10 Å in the orthorhombic form at 295 K. Considering the sum of ionic radii, $Na^+ + O^{2-}$ (=2.79 Å) [35], the coordination number of an Na was supposed to be 7 or 7+5 in orthorhombic NKN. In tetragonal NKN at 474 K, the Na atom was surrounded by 8 O at 2.74–2.81 Å and extra 4 O at 2.91 Å. In cubic NKN at 674 K, the Na atom was surrounded by 8 O at 2.70–2.83 Å and extra 4 O at 2.94 Å. The Na–O distances in each form were less affected by temperature, considering their estimated standard uncertainties.

Therefore, it was concluded that the coordination number of an Na was always small compared with K in orthorhombic,

tetragonal and cubic forms, and that it had an increasing tendency upon heating, i.e., 7+5 in orthorhombic to 8+4 in tetragonal and cubic. Since the O–T/T–O transition was accompanied by changes in coordination number of both Nb and Na, its transition mechanism was supposedly more complicated than the T–C/C–T transition. In another point of view, this would allow room for tuning the O–T/T–O transition behaviours in practical applications by appropriate doping at the alkaline sites as well as the niobium sites.

3.7. Changes in spontaneous polarisation

The spontaneous polarisation (P_s) can be estimated from

$$P_s = \{cS/V\}e,$$
$$S = \sum_i^{cell} Q_i \delta z_i,$$

using charges Q_i of atom i, fractional shifts δz_i from the reference point along the polar axis $\boldsymbol{c}$, unit cell volume V and elementary electric charge e ($=1.602\times10^{-19}$ C) [37].

The composition $KNaNb_2O_6$ ($Z=2$) in the orthorhombic form can be rewritten as $NaO_{0.5}+KO_{0.5}+2Nb_1O_{2.5}$, using single oxide components, each of which retains charge neutrality. In the *Bmm*2 structure, the K atom was coordinated to eight O1 and four O2 atoms (12-fold coordination); the Nb atom was coordinated to four O1 and two O2 atoms (6-fold octahedral coordination), as shown in Fig. 1. Although Na was found to have smaller coordination number than K as mentioned in Section 3.6, contributions from all 12 O were considered in the P_s calculation for simplification. Considering this structural information, the composition could be further modified as

$$NaO_{0.5}+KO_{0.5}+2Nb_1O_{2.5} = Na\left(\frac{1}{24}\right)(O1_8O2_4) + K\left(\frac{1}{24}\right)(O1_8O2_4)+2\left\{Nb\left(\frac{10}{24}\right)(O1_4O2_2)\right\}.$$

Therefore, the total P_s could be resolved into three components

$$P_s(\text{total}) = P_s(KO_{0.5})+P_s(NaO_{0.5})+2P_s(NbO_{2.5})$$

where

$$P_s(KO_{0.5}) = \left\{(+1)\delta z(K)+(-2)\left(\frac{8}{24}\right)\delta z(O1) +(-2)\left(\frac{4}{24}\right)\delta z(O2)\right\}c_o\frac{e}{V_o},$$
$$P_s(NaO_{0.5}) = \left\{(+1)\delta z(Na)+(-2)\left(\frac{8}{24}\right)\delta z(O1) +(-2)\left(\frac{4}{24}\right)\delta z(O2)\right\}c_o\frac{e}{V_o},$$
$$P_s(NbO_{2.5}) = \left\{(+5)\delta z(Nb)+(-2)\left(\frac{40}{24}\right)\delta z(O1) +(-2)\left(\frac{20}{24}\right)\delta z(O2)\right\}c_o\frac{e}{V_o}.$$

In the tetragonal structure, the K atom was coordinated to four O1 and eight O2 atoms (12-fold coordination); the Nb atom was coordinated to two O1 and four O2 atoms (6-fold coordination) (Fig. 1). The Na atom was assumed to have the same coordination as K, in a similar way to the orthorhombic case. Considering this structural information, the composition of an $Na_{0.5}K_{0.5}NbO_3$ in a unit cell could be written as

$$\frac{1}{2}NaO_{0.5}+\frac{1}{2}KO_{0.5}+Nb_1O_{2.5} = \frac{1}{2}\left\{Na\left(\frac{1}{24}\right)(O1_4O2_8)\right\} + \frac{1}{2}\left\{K\left(\frac{1}{24}\right)(O1_4O2_8)\right\}+Nb\left(\frac{10}{24}\right)(O1_2O2_4).$$

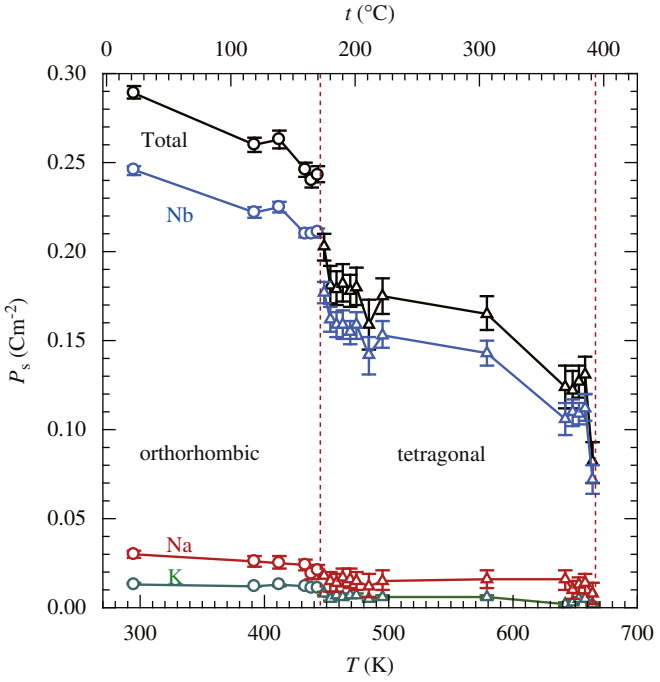

Fig. 5. Temperature dependence of spontaneous polarisation (P_s) with estimated standard uncertainties in the orthorhombic (○) and tetragonal (Δ) forms of $Na_{0.5}K_{0.5}NbO_3$ upon cooling. Contributions from the monoxide components, $NbO_{2.5}$, $KO_{0.5}$ and $NaO_{0.5}$, are also shown in addition to the total P_s.

The total P_s could then be expressed as the sum of three monoxide components

$$P_s(\text{total}) = \frac{1}{2}P_s(KO_{0.5})+\frac{1}{2}P_s(NaO_{0.5})+P_s(NbO_{2.5})$$

where

$$P_s(KO_{0.5}) = \left\{(+1)\delta z(K)+(-2)\left(\frac{4}{24}\right)\delta z(O1) +(-2)\left(\frac{8}{24}\right)\delta z(O2)\right\}c_t\frac{e}{V_t},$$
$$P_s(NaO_{0.5}) = \left\{(+1)\delta z(Na)+(-2)\left(\frac{4}{24}\right))\delta z(O1) +(-2)\left(\frac{8}{24}\right)\delta z(O2)\right\}c_t\frac{e}{V_t},$$
$$P_s(NbO_{2.5}) = \left\{(+5)\delta z(Nb)+(-2)\left(\frac{20}{24}\right)\delta z(O1) +(-2)\left(\frac{40}{24}\right)\delta z(O2)\right\}c_t\frac{e}{V_t}.$$

The changes in P_s with decreasing temperature are shown in Fig. 5. Typical values of P_s in the orthorhombic and tetragonal forms were *ca.* 0.29 C m^{-2} at 300 K and 0.18 C m^{-2} at 460 K, respectively. The P_s gradually decreased with increasing temperature and fell discontinuously near the transition points. The difference in P_s between the heating and cooling procedures was small.

Although the total P_s consisted predominantly of the Nb oxide component, small, but significant, contributions from the Na and K components were recognized in the orthorhombic and tetragonal forms. The Na component was slightly larger than the K component by the reason mentioned in Section 3.1. The sum of the fractions of Na and K contributions to the total P_s was estimated to be *ca.* 15%.

Hewat estimated the values of P_s for the orthorhombic and tetragonal forms of KN at 0.36 and 0.33 C m^{-2} from the structural data [38]. On the other hand, Michel-Calendinit and Chermettez estimated them at 0.35 and 0.28 C m^{-2} by the self-consistent-field multiple-scattering Xα method [39]. The P_s values for NKN estimated in the present study were slightly small compared with KN, as was expected from $[c/a-1]$, i.e., 1.1% for NKN and 1.7% for KN [40]. Experimental data for the P_s of NKN varied in the range between 0.2 and 0.3 C m^{-2} in the literature; for example, Du et al. reported a *D*–*E* hysteresis curve for various Bi_2O_3-doped NKN, in which the non-doped orthorhombic NKN had a P_s value of *ca.* 0.22 C m^{-2} [41]. The present result essentially agreed with previous studies, allowing the relatively large uncertainties associated with difficulties in the experiments and method.

3.8. Dielectric and thermal properties

The dielectric constant (ε') is plotted as a function of temperature in Fig. 6. The dielectric constant peaked at *ca.* 10,000 near the C–T phase transition point under the applied frequency of 10 kHz. The transition temperatures were estimated from the $1/\varepsilon$ vs. *T* plot, as 457 K for O–T and 668 K for T–C upon heating, and 432 K for T–O and 652 K for C–T upon cooling. No significant differences were observed in the estimated transition points measured at different frequencies.

The dielectric losses (tan δ) at 10 and 100 kHz are plotted as a function of temperature in Fig. 7. Upon heating, the dielectric loss fell sharply near the O–T transition, whereas it formed a sharp peak near the T–C transition. Upon cooling, however, it formed a relatively low peak near the C–T and T–O transitions. Although the dielectric losses at 0.1 and 1 kHz were much larger than those measured at 10 and 100 kHz, they still clearly indicated the presence of phase transitions. The phase transition temperatures are summarised in Table 2, including data from the recent literature [36].

The results of the DSC measurements near the O–T and T–C phase transitions upon heating are shown in Fig. 8. The endothermic peak associated with the O–T transition had a W-shaped profile between 458 and 480 K with two minima at 466 and 475 K. In regard to the T–C transition, there was a sharp endothermic depression commencing at 689 K, which was preceded by a broad endothermic depression between 662 and 683 K. If we combined these two depressions and assumed a rather deformed W-shaped endothermic peak, then the T–C transition could be estimated to commence at 662 K. The X-ray discontinuities corresponded to the first (lower) minima of the W-shaped peaks in both transitions, though we had no clear explanation for the deformed DSC profiles.

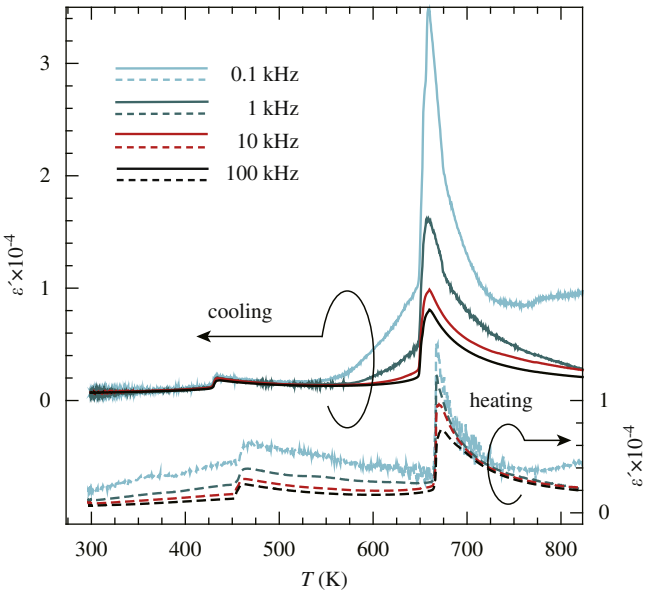

Fig. 6. Changes in dielectric constant (ε') with temperature upon heating (dashed lines) and cooling (solid lines); as measured at 0.1, 1, 10 and 100 kHz.

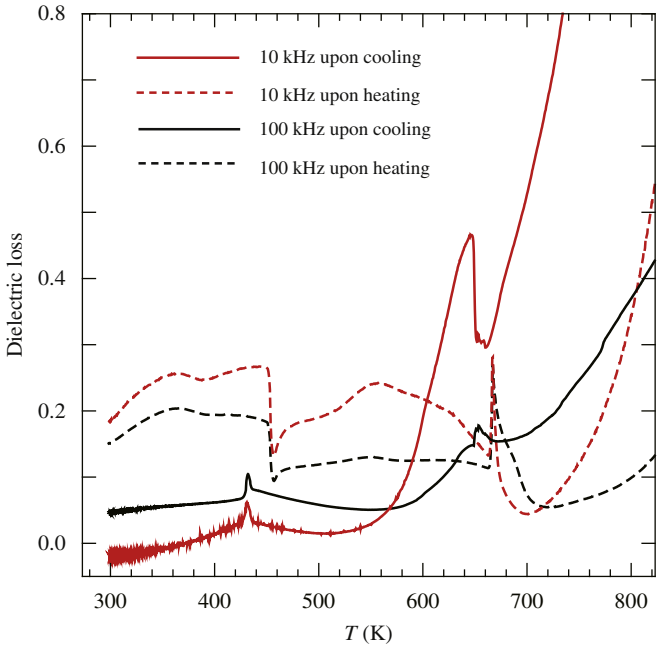

Fig. 7. Changes in dielectric loss (tan δ) with temperature upon heating (dashed lines) and cooling (solid lines); as measured at 10 kHz (red) and 100 kHz (black). (For interpretation of the references to colour in this figure legend, the reader is referred to the web version of this article.)

4. Conclusions

Single-crystals of sodium potassium niobate $Na_{0.5}K_{0.5}NbO_3$ were grown by the flux method, using a KF–NaF eutectic mixture. The *in-situ* high-temperature single-crystal diffraction experiments revealed the structural evolution associated with two transitions between O and T, and T and C. Upon heating, the pseudocubic unit cell volume collapsed discontinuously at these transition points, whereas the reverse took place upon cooling. The transition temperatures were estimated from the discontinuities as 465 K for O–T and 671 K for T–C during heating and 446 K for T–O and 666 K for C–T during cooling. All these features suggested that both transitions were of the first order.

The coordination numbers of the Nb atom in three forms could be considered to have a decreasing tendency with decreasing temperature (i.e., 6 in cubic, 5+1 in tetragonal and 4+2 in orthorhombic). In the orthorhombic and tetragonal ferroelectric forms, the Na and K atoms occupied slightly different positions along the polar axis. In the cubic form, the Na atoms were distributed statistically at slightly displaced positions from the ideal sites occupied by the K atoms. The coordination number of the Na atom was always small compared with K at all temperatures investigated, and showed an increasing tendency upon heating, i.e., 7+5 in orthorhombic to 8+4 in tetragonal and cubic forms. Since the O–T/T–O transition was accompanied by changes in coordination number of both Nb and Na, the transition mechanism was supposedly more complicated than the T–C/C–T transitions.

Table 2
Estimated phase transition temperatures for $Na_{0.5}K_{0.5}NbO_3$.

Sample	Method	O–T on heating (K)	T–O on cooling (K)	T–C on heating (K)	C–T on cooling (K)
Single	X-ray	465	446	671	666
Single	DSC	458		662	
	ε	457	432	668	652
	tan δ	454	432	667	650
10 μm grain ceramics[a]	DSC	464.2		677	
	ε		452		667
0.5 μm grain ceramics[a]	DSC	456.7		672.7	
	ε		460		654

[a] Buixaderas et al. [36].

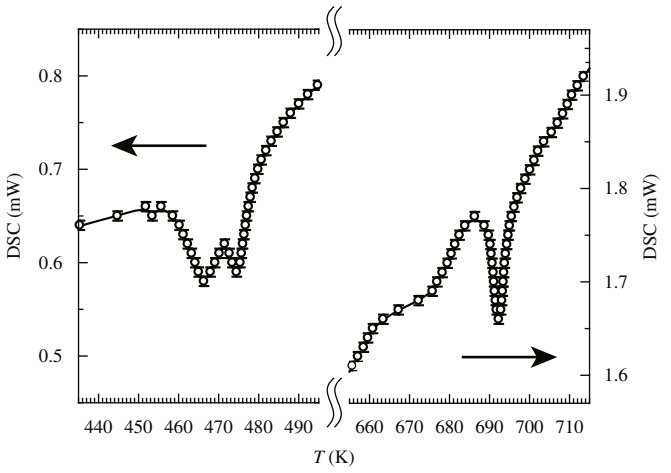

Fig. 8. Differential scanning calorimetry upon heating at the rate of 10 K/min near the orthorhombic-tetragonal (left) and tetragonal-cubic (right) transitions.

The magnitudes of P_s estimated from the atom positions and formal charges were *ca.* 0.29 C m^{-2} in the orthorhombic form and *ca.* 0.18 C m^{-2} in the tetragonal form. The contribution of the alkaline oxide components to the total P_s was estimated to be approximately 15% in both forms. The difference in ionic sizes between Na and K gave the Na atom an attribute of rattling in the cavity surrounded by the corner-sharing NbO_6 octahedra. The small Na not only vibrated with large amplitude, but also shifted further from the centre of the cavity than K, resulting in a larger contribution to the total polarisation in the ferroelectric forms.

The transitions were also manifested in the temperature dependency of the dielectric properties measured at 0.1, 1, 10 and 100 kHz. The DSC analysis suggested the presence of W-shaped endothermic peaks having two minima at each transition upon heating. The first (lower) minima of the endothermic peaks approximately corresponded to the discontinuities observed by the X-ray diffraction.

Acknowledgments

The authors are grateful to Mr. Masashi Koide for dielectric measurements. This work was supported by the Grant-in-Aids for Scientific Research nos. 1820671 and 22360272 from the Japan Society for the Promotion of Science. JW and TS appreciate the research assistant scholarships from the Institute of Ceramics Research and Education, Nagoya Institute of Technology, and YI appreciates the Research Fellowship from the Japan Society for the Promotion of Science for Young Scientists.

Appendix A. Supplementary material

Supplementary data associated with this article can be found in the online version at doi:10.1016/j.jssc.2010.09.018.

References

[1] Y. Saito, H. Takao, T. Tani, T. Nonoyama, K. Takatori, T. Homma, T. Nagaya, M. Nakamura, Nature 432 (2004) 84–87.
[2] Y.P. Guo, K. Kakimoto, H. Ohsato, Appl. Phys. Lett. 85 (2004) 4121–4123.
[3] M. Ahtee, A.M. Glazer, Acta Crystallogr. A 32 (1976) 434–446.
[4] D.W. Baker, P.A. Thomas, N. Zhang, A.M. Glazer, Acta Crystallogr. B 65 (2009) 22–28.
[5] E.A. Wood, Acta Crystallogr. 4 (1951) 353–362.
[6] L. Katz, H.D. Megaw, Acta Crystallogr. 22 (1967) 639–648.
[7] A.W. Hewat, J. Phys. C: Solid State Phys. 6 (1973) 2559–2572.
[8] M. Ahtee, A.W. Hewat, Acta Crystallogr. A 34 (1978) 309–317.
[9] T.A. Skidmore, T.P. Comyn, S.J. Milne, Appl. Phys. Lett. 94 (2009)) 222902.
[10] ICSD: Inorganic Crystal Structure Database, 2010.1, Fachinformationszentrum Karlsruhe, Germany, 2010.
[11] B.T. Matthias, J.P. Remeica, Phys. Rev. 82 (1951) 727–728.
[12] L. Lian, T.C. Chong, H. Kumagai, M. Hirano, L. Taijing, S.C. Ng, J. Appl. Phys. 80 (1996) 376–381.
[13] Y. Inagaki, K. Kakimoto, Appl. Phys. Express 1 (2008)) 061602.
[14] K.G. Deshmukht, S.G. Ingle, J. Phys. D: Appl. Phys. 4 (1971) 1633–1636.
[15] E. Wiesendanger, Czech. J. Phys. B 23 (1973) 91–99.
[16] J. Fousek, Czech. J. Phys. B 21 (1971) 955–968.
[17] G. Metrat, L. Mayet, M.D. Fontana, J.L. Servoin, Ferroelectrics 55 (1984) 215–218.
[18] V. Gopalan, R. Raj, J. Am. Ceram. Soc. 79 (1996) 3289–3296.
[19] J. Hirosaki, K. Yamada, H. Kamio, S. Shichijyo, Jpn. J. Appl. Phys. 43 (2004) 2396–3289.
[20] N. Lu, R. Yu, Z. Cheng, Y. Dai, X. Zhang, J. Zhu, Appl. Phys. Lett. 96 (2010) 221905.
[21] P.R. Comes, M. Lambert, A. Guinier, Solid State Commun. 6 (1968) 715–719.
[22] M. Lambert, R. Comes, Solid State Commun. 7 (1969) 305–308.
[23] P.R. Comes, M. Lambert, A. Guinier, Acta Crystallogr. A 26 (1970) 244–254.
[24] H. Krakauer, R. Yu, C.-Z. Wang, J. Phys. Chem. Solids 57 (1996) 1409–1412.
[25] V.A. Shuvaeva, K. Yanagi, K. Yagi, K. Sakaue, H. Terauchi, Solid State Commun. 106 (1998) 335–339.
[26] B. Ravel, E.A. Stern, R.I. Vedrinskii, V. Kraizman, Ferroelectrics 206 (1998) 407–430.
[27] M. Sepliarsky, M.G. Stachiotti, R.L. Migoni, C.O. Rodriguez, Ferroelectrics 234 (1999) 9–27.
[28] H. Krakauer, R. Yu, C.-Z. Wang, K.M. Rabe, U.V. Waghmare, J. Phys.: Condens. Matter 11 (1999) 3779–3787.
[29] R. Blinc, J. Seliger, B. Zalar, Integrated Ferroelectrics 61 (2004) 255–260.
[30] N. Ishizawa, S. Kondo, H. Hibino, S. Igarashi, M. Nakamura, R. Saho, Annual report of ceramics research laboratory 2006, Nagoya Inst. Technol. 6 (2007) 12–18.
[31] B.B. He, U. Preckwinkel, Adv. X-ray Anal. 45 (2002) 332–337.
[32] Bruker, SAINT, Smart Apex II, Bruker AXS Inc., Madison, Wiskonsin (2007).
[33] G.M. Sheldrick, Acta Crystallogr. A 64 (2008) 112–122.
[34] L.J. Farrugia, J. Appl. Crystallogr. 32 (1999) 837–838.
[35] R.D. Shannon, Acta Crystallogr. A 32 (1976) 751–767.
[36] E. Buixaderas, V. Bovtun, M. Kempa, M. Savinov, D. Nuzhnyy, F. Kadlec, P. Vaněk, J. Petzelt, M. Eriksson, Z. Shen, J. Appl. Phys. 107 (2010) 014111.
[37] T. Nakamura, Ferroelectrics and Structural Phase Transition (in Japanese), Shokabou, Tokyo, 1988.
[38] A.W. Hewat, J. Phys. C: Solid State Phys. 6 (1973) 1074–1084.
[39] F.M. Michel-Calendinit, H. Chermettez, J. Phys. C: Solid State Phys. 14 (1981) 1179–1192.
[40] G. Shirane, A. Newnham, R. Pepinsky, Phys. Rev. 96 (1954) 581–588.
[41] H. Du, D. Liu, F. Tang, D. Zhu, W. Zhou, S. Qu, J. Am. Ceram. Soc. 90 (2007) 2824–2829.